Published in final edited form as:
Mass Spectrom Rev. 2010 ; 29(2): 294–312. doi:10.1002/mas.20232.

The Ion Funnel: Theory, Implementations, and Applications

Ryan T. Kelly, **Aleksey V. Tolmachev**, **Jason S. Page**, **Keqi Tang**, and **Richard D. Smith**[*]
Biological Sciences Division, Pacific Northwest National Laboratory, P.O. Box 999, Richland, WA 99352

Abstract

The electrodynamic ion funnel has enabled the manipulation and focusing of ions in a pressure regime (0.1 to 30 Torr) that has challenged traditional approaches, providing the basis for much greater mass spectrometer ion transmission efficiencies. The initial ion funnel implementations aimed to efficiently capture ions in the expanding gas jet of an electrospray ionization source and radially focus them for efficient transfer through a conductance limiting orifice. We review the improvements in fundamental understanding of ion motion in ion funnels, the evolution in its implementations that have brought the ion funnel to its current state of refinement, as well as applications of the ion funnel for purposes such as ion trapping, ion cooling, low pressure electrospray, and ion mobility spectrometry.

Keywords

ion optics; rf focusing; ion guide; multipole ion guide; stacked ring ion guide; ESI

I. INTRODUCTION

The prominent and rapidly expanding role of mass spectrometry (MS) in the physical and biological sciences can be attributed in part to the versatility afforded by the growing catalog of available ionization methods. Many ionization techniques of increasing importance operate at elevated or atmospheric pressure, including electrospray ionization (ESI) (Fenn et al., 1990), atmospheric pressure matrix-assisted laser desorption/ionization (AP MALDI) (Creaser & Ratcliffe, 2006), and desorption electrospray ionization (DESI) (Takats et al., 2004). To achieve the maximum possible sensitivity, ions created at higher pressures must be transmitted with high efficiency through narrow, conductance limiting apertures that separate differentially pumped vacuum chambers prior to reaching the high vacuum region of the mass analyzer. The extent to which the motion of ions can be controlled in these different vacuum stages largely determines the overall ion transmission efficiency of the mass spectrometer.

In the absence of background gas molecules (e.g., high vacuum), ions can be manipulated with extreme precision and in a well understood fashion using magnetic and electric fields. At elevated pressures, collisions with gas molecules increasingly dominate the behavior of ion motion. Such collisions have been successfully exploited at lower pressures (~10 mTorr) since at least the early 1990s, where collisional ion focusing within rf-only multipoles ensures efficient transmission to high vacuum (Thomson, 1998). At higher pressures (~1 Torr and above), it becomes much more challenging to control ion motion over larger areas or volumes, particularly in the presence of strong gas dynamic effects that typically occur in the first vacuum stage of a mass spectrometer, as conventional ion optics become ineffective

[*]Corresponding Author. email: rds@pnl.gov .

at these higher pressures. For example, the high rate of collisions inhibits effective focusing with static lens stacks, and rf-only multipoles exhibit either an acceptance area that is too small to efficiently capture ions from an expanding gas jet (for small inscribed radius) or an effective potential that is too weak to focus ions to a narrow conductance-limiting aperture (for large inscribed radius). As a result, nearly all commercial mass spectrometers have conventionally employed a skimmer as a conductance-limiting orifice to separate the first and the second vacuum chambers, which samples only a small fraction of the ion cloud and creates a major sensitivity bottleneck for MS.

The ion funnel was originally implemented in our laboratory (Shaffer et al., 1997) as a replacement for the ion transmission-limited skimmer, seeking to efficiently capture ions entering the first (rough pumped) vacuum stage from an ESI source to ensure their near lossless transmission through a conductance-limiting orifice. Since its creation, the ion funnel has been adapted for a variety of uses and has proven to be a broadly applicable tool for ion focusing and manipulation at elevated pressures that challenge conventional approaches. Although it has undergone several iterations since it was conceived, the defining features of the ion funnel are a series of closely spaced ring electrodes whose inner diameters gradually decrease, serving to radially confine ions as they pass through. Out-of-phase rf potentials are applied to adjacent electrodes, and a dc gradient is typically applied along the axis of the ion funnel to drive ions through the device.

In this review, we describe the concept of the ion funnel and detail the improvements in hardware design that have led to dramatically improved performance, as well as the computer modeling that has provided a clearer understanding of ion funnel operation. The applications of the ion funnel are then discussed, which not only encompass the original aim of improving ion transmission through ESI-MS interfaces, but also include ion mobility spectrometry (IMS), ion cooling for nuclear physics applications, low-pressure electrospray, ion trapping and more. We also briefly discuss other related ion optic designs and approaches that seek to achieve similar results as the ion funnel.

II. PRINCIPLE OF OPERATION

The ion funnel is related to the stacked ring rf ion guide (Gerlich, 1992), which consists of a series of cylindrical ring electrodes of fixed i.d. (Figure 1). Radio frequency potentials of opposite polarity are applied on adjacent electrodes. The arrangement creates an effective potential (also called pseudo-potential) that radially confines ions inside the ion guide. The effective potential, V^*, expressed in *Volts*, is proportional to the squared amplitude of the local rf electric field E_{rf} (Dehmelt, 1967; Gerlich, 1992):

$$V^*(r,z) = \frac{z_i e \left| E_{rf}(r,z) \right|^2}{4m\omega^2} \tag{1}$$

Here z_i and e are ion charge state and elementary charge, respectively, m is the ion mass in SI units, and ω is the rf frequency f expressed in angular units, $\omega = 2\pi f$. The radial and axial positions are represented by r and z, respectively (Figure 1). The stacked ring geometry generates the electric field configuration that corresponds to the following effective potential spatial distribution (Gerlich, 1992;Tolmachev et al., 2000):

$$V^*(r,z) = V_{\text{trap}} \left[I_1^2(r/\delta) \cos^2(z/\delta) + I_0^2(r/\delta) \sin^2(z/\delta) \right] \tag{2}$$

$$V_{\text{trap}} = \frac{V_{\max}}{I_0^2(\rho/\delta)}; \quad V_{\max} = \frac{z_i e V_{rf}^2}{4m\omega^2\delta^2} \tag{3}$$

V_{trap} is the axial effective potential well depth; V_{max} is the maximum value of the effective potential at $r = \rho$, $z = d(i+1/2)$, $i=0,1,\ldots$; d is the spacing between the ring electrodes; I_0, I_1 are zero and 1st order modified Bessel functions, respectively; $\delta = d/\pi$; V_{rf} is one half of the peak-to-peak rf amplitude. The stacked ring rf ion guide creates an effective potential distribution that corresponds to a steep potential gradient near the electrodes and a near field free region over most of the internal volume.

The ion funnel was based on the stacked ring rf ion guide, but utilized ring electrodes with progressively smaller i.d.'s, enabling the spatially dispersed ion cloud entering the ion funnel to be efficiently focused to a much smaller radial size for efficient transfer through the conductance limiting orifice at the exit (Shaffer et al., 1997). The device was originally intended for operation in the high pressure region of the ESI-MS interface, typically 1 to 10 Torr, compared to pressures below 0.1 Torr used previously with stacked ring ion guides and in general with rf ion guides of any geometry. Another important new feature of the ion funnel was the dc potential gradient applied to the ring electrodes to drive ions along the axis, which provided added control relative to relying solely on gas dynamic effects (Shaffer et al., 1999). This feature took advantage of the fact that the stacked ring ion guide geometry is naturally "segmented" in the axial direction, in contrast to the axial continuity of standard multipoles. Multiple studies of the ion funnel have explored the properties of the ion funnel in various applications, as reviewed in the sections below.

III. EVOLUTION OF THE ION FUNNEL

While the ion funnel concept continues to be adapted to a growing number of applications (see Section IV), its original and most prevalent use has been to decrease the ion losses that occur in the interface of high pressure ion sources of mass spectrometers. In this section, the successive refinements that have been applied to the ion funnel over the past decade to increase ESI-MS sensitivity are detailed. Other devices that aim to employ rf focusing for the same purpose are reviewed as well.

A. Hardware Improvements

The first published ion funnel design (Shaffer et al., 1997), shown in Figure 2, consisted of 28 electrodes (rings, lenses) that decreased in i.d. from 22 mm to 1.0 mm. Each of the ion funnel rings was 1.59 mm thick, and the ceramic spacers inserted between them had the same thickness. Carbon resistors were soldered between neighboring electrodes to enable a linear dc potential gradient, and capacitors were utilized to decouple the rf and dc power sources. Initial coupling of this ion funnel with a mass spectrometer demonstrated >10-fold signal gains relative to the unmodified instrument, but a significant *m/z* bias in the mass spectra was evident. For example, while dramatic gains in sensitivity were observed for peaks between *m/z* 800 and 1000, peaks below *m/z* 750 and above *m/z* 1250 were almost completely rejected. This relatively narrow transmission window could be shifted to higher or lower values by varying the applied rf potentials, but simultaneous ion transmission over a broad *m/z* range was not possible with this design.

Computational modeling (see Section IIIB) indicated that the *m/z*-dependent ion transmission behavior of the initial ion funnel was due to pronounced axial rf potential wells that form at the exit of the ion funnel when the orifice is small relative to the interelectrode

spacing (Shaffer et al., 1999). Therefore, in the subsequent prototype the i.d. of the final ion funnel ring was increased from 1.0 mm to 2.0 mm (Shaffer et al., 1999). This small design modification significantly reduced ion transmission biases, but maximum signal enhancement was still achieved when the rf amplitude was optimized for each analyte. Since the optimum rf amplitude was found to increase approximately linearly with increasing *m/z*, the authors sought to further broaden the transmission window using a linked scan of rf voltage with the quadrupole mass analyzer. Using this approach the charge state distribution for a model protein was found to be very similar to that obtained with the skimmer interface, but with more than an order of magnitude intensity increase. Despite its effectiveness, linked scanning of the rf potential with the mass analyzer has some notable limitations. The approach is only applicable to certain mass analyzers such as those employing quadrupole mass filters, and cannot be applied to other mass analyzers for which ion introduction and analysis are decoupled. Further, because ion activation also increases with increasing rf voltage, ion fragmentation can occur at high rf, leading to artifacts in the mass spectra.

To overcome these difficulties, Kim et al. (2000a) developed a new design that, aside from a few noteworthy modifications that have since been incorporated, closely resembles ion funnels that are currently in use. The electrodes were made from 0.5-mm-thick brass plates, and the dielectric spacers inserted in between electrodes were 0.5-mm-thick patterned Teflon sheets. Each of the brass plates had tabs that were used for electrical connection via zero-insertion-force (ZIF) sockets. A custom-made circuit board with a resistor chain was mounted onto a ZIF socket to provide the dc gradient. On the other side of the funnel, a second ZIF socket was connected to a circuit board with two capacitor networks for providing rf to each electrode, with neighboring plates 180° out of phase from one another. The total number of electrodes increased from 28 to 100 for the new design, with the first 55 electrodes having a constant i.d. of 25.4 mm, and the final 45 electrodes tapering in uniform steps to a 1.5-mm-i.d. conductance-limiting electrode. The fixed-diameter section increased residence time to enhance droplet and cluster desolvation, and also helped to disperse the directed gas flow from the inlet capillary prior to reaching the ion funnel exit. While partially effective, enhanced pumping was still needed; a high speed roots pump was connected to the ion funnel chamber, and an additional turbo pump was used in the octopole region of the mass spectrometer. Because of the closer spacing between neighboring electrodes relative to the i.d. of the exit plate, the axial pseudopotential well depth that had hindered transmission of low *m/z* species was further reduced, such that it was no longer necessary to scan the rf voltage with the quadrupole to achieve broad, unbiased *m/z* transmission. This was fortunate, not only for simplifying the supporting electronics, but because the ion funnel could be more broadly applied beyond mass filter-based instruments. For example, this design was used in the first implementation of the ion funnel with an FTICR instrument (Belov et al., 2000a; Belov et al., 2000b), and helped to achieve the lowest detection limits reported to date for ESI-MS (~30 zmol or ~18,000 molecules).

Early work with the ion funnel recognized that due to gas dynamic effects the pressure in the ion funnel vacuum chamber was not uniform; the effective pressure at the ion funnel exit was estimated to be 2–3 times higher than the value recorded at the pressure gauge (Shaffer et al., 1998), leading to increased pumping requirements in downstream vacuum chambers. This was because although the expanding supersonic gas jet entering the chamber terminates at the Mach disk just a few mm from the capillary exit, a significant amount of directed flow persists a much greater distance (Douglas & French, 1988; Tejeda et al., 1996), even to the exit of the ion funnel. Efforts to reduce these effects such as increasing the length of the ion funnel by adding a fixed width drift region (Kim et al., 2000a) were only partially successful; additional high speed pumps were required in all previous designs. This directed gas flow became especially problematic as efforts to increase ion transmission into the ion funnel chamber led to the use of larger i.d. (Kim et al., 2000a) or multiple (Kim et al.,

2000b) inlets, creating correspondingly greater gas loads. Kim, et al. (2001) developed an effective approach to mitigate these gas dynamic effects by disrupting the gas flow in the ion funnel. A 9-mm-diameter brass disk, termed the “jet disrupter” electrode, was suspended perpendicular to the gas flow in the center of the ion funnel, 22 mm downstream of the first ion funnel electrode to effectively block the “line of sight” between the inlet and the conductance limit. The jet disrupter was suspended by two thin wires connected to a ring electrode, which allowed a dc voltage to be applied with no rf. By biasing the jet disrupter ~5 V above adjacent ring electrodes, ions were deflected around the electrode while the gas molecules were effectively dispersed and evacuated by the pump on the ion funnel chamber. Current measurements made using a 7-capillary heated inlet and an ion funnel with and without the jet disrupter indicated that ion transmission efficiency was preserved when the jet disrupter was used. Importantly, for a given inlet/pump configuration in the ion funnel chamber, the pressure in the subsequent vacuum chamber was 2–3 times lower when the jet disrupter was employed. This allowed for greater conductance into the ion funnel with a high speed pumping configuration, or alternatively made it possible to operate the ion funnel with a lower pumping speed system. In this work the sensitivity gains for both a 7-capillary inlet and a custom-built orifice inlet having a counter-flow of nitrogen gas were also measured. The interfaces had a similar conductance and produced similar increases in intensity relative to the standard instrument setup. In addition, *S/N* was compared between the ion funnel-modified designs and the standard interface. The ion funnel did not increase *S/N* for MS-only measurements for which “chemical noise” dominated, as the signal from interfering species increased in proportion to the analyte signal, but a clear improvement was shown for MS/MS analyses where such species were removed.

More recently, Page et al. (2007) interfaced an ion funnel with both Thermo LTQ linear ion trap and LTQ-FT hybrid instruments, enabling a direct comparison of performance with the unmodified instruments for proteomics analyses. This version was similar to that initially developed by Kim et al. (2000a), but incorporated refinements in design and fabrication that had been made over time, including a jet disrupter electrode, as shown in Figure 2. The electrode rings were created by electrical discharge machining rather than boring a tapered hole through a stack of electrodes, which improved reproducibility and eliminated the need for manually removing burrs from each plate. The jet disrupter enabled the standard rough pump supplied with the LTQ to maintain the ion funnel chamber at a useful pressure (~1.3 Torr). With the latest design incorporated onto LTQ ion trap instruments, the authors found that the accumulation time required to “fill” the trap was reduced by 90%. For MS-only experiments, the effect on instrument performance was minimal, as the fill time accounted for a relatively small portion of the overall duty cycle; however, MS/MS experiments required longer ion accumulation times for the selected ions, and the ion funnel provided a significant benefit. For example, for the smallest samples (0.3 μg) of *S. Oneidensis* tryptic digest analyzed by LC-MS/MS, the ion funnel-modified LTQ produced twice the number of peptide identifications relative to the standard instrument. Figure 3 compares base peak chromatograms of the *S. Oneidensis* digest obtained using the LTQ with (A) a standard skimmer interface and (B) an ion funnel interface. Not only is the dramatic (~7-fold) sensitivity increase apparent when the ion funnel is employed, but the similar profiles in the chromatograms and mass spectra (Figures 3C and 3D) highlight the absence of *m/z* bias in ion transmission. The ion funnel was also evaluated in a LTQ-FT hybrid ion trap-FTICR instrument. Because of the greater ion populations utilized by the hybrid instrument (requiring longer ion accumulation times), the ion funnel provided a larger improvement in duty cycle (~25– 55%) than for the standalone ion traps.

B. Insights from Theoretical Modeling

At pressures exceeding 1 Torr, with ion mean free paths on the order of 1 μm, the large number of ion-neutral collisions results in ion motion that can no longer be described by the governing equations in vacuum that are regularly applied for dc and rf ion optics design. Also, the ion funnel generally utilizes an axial dc electric field to facilitate ion motion through the dense gas medium, an approach essentially new for rf ion guides when first implemented (Shaffer et al., 1997). Ion funnel development was thus accompanied by computer modeling that enhanced the understanding of ion optical properties and guided refinements in design. The first report on the initial ion funnel prototype included results of simulations performed with a users program written for SIMION (Scientific Instrument Services, Ringoes, NJ) to model the effects of rf fields and viscous damping of gases (Shaffer et al., 1997). The approach, though qualitative, provided a picture of ion motion governed by a combination of effective rf focusing, the axial dc field and the viscous damping forces from the bath gas. The observed narrow *m/z* window of the original prototype (Shaffer et al., 1997; Shaffer et al., 1998) was initially difficult to interpret, however, as the simplified computer model available at the time suggested 100% ion transmission efficiency for *m/z* as low as 18 for a wide range of rf, dc and pressure conditions modeled (Shaffer et al., 1997).

To improve the ion funnel performance, it was necessary to develop an adequate theoretical understanding of its ion transmission properties. The effort began with the creation of a computer model that was capable of a realistic representation of all major aspects of the ion funnel operation (Tolmachev et al., 2000). The model was created based on previously developed modeling and theoretical approaches for collisional cooling and focusing rf ion guides (Douglas & French, 1992; Dodonov et al., 1997; Tolmachev et al., 1997). Four major components were considered. First, the damping action of the ion-neutral collisions was included at the quantitative level, based upon experimental and theoretical studies of collisional cooling. Second, a realistic model of the random component of the ion-neutral collisions was incorporated; the process was previously found to be essential for obtaining a correct scale of the ion focusing in collisional focusing ion guides (Tolmachev et al., 1997). Third, rf focusing was simulated at the rf ion motion time scale, rather than using an effective potential approximation. This detailed level of ion motion simulations required sub-microsecond time steps, which greatly increased computation time. However, modeling the fast rf motion of ions was necessary to correctly predict low *m/z* ion transmission behavior and also to quantitatively describe ion losses in the narrow ion funnel exit. Even more important, a realistic behavior with respect to gas pressure could only be obtained when the ion motion was simulated completely, down to the scale of rf oscillations. Finally, the new model included a simulation of the coulombic ion-ion interactions, which defined the spatial distribution of ions inside the ion funnel and was found to be critical for obtaining correct ion transmission characteristics. The space charge forces were simulated using the macro-ion multi-particle approach (Tolmachev et al., 2000), which further increased the computational intensity of the model.

The model demonstrated behavior consistent with the experimental results (Shaffer et al., 1999), such that the reduced ion transmission efficiency and *m/z*-dependent optimum rf voltage were reproduced. The model showed that ions can be trapped in effective potential wells created along the ion funnel axis at z-positions corresponding to each exit ring electrode. The axial wells trap ions in an *m/z*-dependent fashion, creating the undesired *m/z*-dependent transmission behavior. In other words, the traps are filled with ions until fully compensated by space charge potential, which creates radial fields, resulting in the ion ejection and loss in the radial direction. This led to the increase in exit ring diameters from 1 mm to 2 mm (Shaffer et al., 1999). While this increase in diameter indeed reduced the unwanted axial potential traps, the trapping effect was still quite severe, as seen from the

calculated effective potential distribution for the modified configuration (Figure 4). The effective potential was calculated based on the rf electric field intensity $E_{rf}(r, z)$, computed numerically for the dimensions of the updated ion funnel using eq. (1). The largest axial well, indicated by an arrow in Figure 4, is quite pronounced and reaches several volts in both the radial and the axial dimensions. The calculation does not include the dc gradient, typically 10 to 30 V/cm, which should be added to the effective potential distribution to obtain the complete picture of the electric fields acting on an ion. Even with the dc field applied, the traps at the exit cannot be fully compensated. The trap effective potential is inversely proportional to *m/z*, thus low *m/z* ions are subject to stronger axial trapping. However, the effective potential, eq. (1), is only applicable for sufficiently high *m/z* for the adiabatic approximation to be valid (Gerlich, 1992). The outcome of this limitation can be easily observed with the model, which shows that low *m/z* ions acquire an increased amplitude of rf oscillations, larger than the size of the axial traps. Such low *m/z* ions cannot be trapped in the axial wells, nor can they be confined by the radial effective focusing since the amplitude of the rf motion becomes too high to fit into the reduced diameters of the exit ring electrodes; the behavior can be termed “low *m/z* instability”. The combination of these two effects defines the *m/z*-dependent ion transmission behavior observed experimentally (section IIIA).

In a separate simulation study, published after the report of the increased exit electrode i.d. (Shaffer et al., 1999), the detrimental action of the axial potential wells was independently confirmed (Lynn et al., 2000). Applying the Douglas ion-neutral collisional drag coefficient model (Chen et al., 1997) into the SIMION ion trajectory simulation package provided insights suggesting opening the exit rings to 2 mm i.d. to minimize axial trapping (Shaffer et al., 1999).

As discussed in section IIIA, a new ion funnel design was developed based upon an increased level of understanding from the improved theoretical modeling. The initial experimental results were published together with the theoretical reasoning (Kim et al., 2000a; Tolmachev et al., 2000), which is briefly summarized below. The computer model generated a time-lapse sequence of ion motion for various conditions. The model clearly demonstrated both the expected ion focusing action and the detrimental effects, such as the low *m/z* instability and trapping in the exit potential wells, providing a way for an intuitive understanding of operation. Eventually, a convenient quantitative description was found in the form of relationships describing ion funnel characteristics. A set of practically useful relationships was obtained for conditions when the inner radius of the ring electrodes, ρ, is large compared to the spacing between electrodes d. The effective potential, V^*, dependence on radius r can be approximated for $d < r < \rho$, as follows:

$$V^*(r) \approx V_\rho^* \frac{\rho}{r} \exp\left(\frac{r-\rho}{\delta/2}\right) \tag{4}$$

Here, $\delta = d / \pi$. The maximum effective potential, corresponding to $r = \rho$, is given by

$$V_\rho^* = \frac{qV_{RF}^2}{4M\omega^2\delta^2} \tag{5}$$

V_{rf} is 0 to peak amplitude of the rf voltage. The axial well depth V_{trap} is given by the following relationships:

$$V_{\text{trap}}=\frac{V_{\rho}^{*}}{I_0^2(\rho/\delta)} \approx V_{\rho}^{*}\cdot 2\pi\frac{\rho}{\delta}\exp\left(-\frac{2\rho}{\delta}\right) \tag{6}$$

In this equation, I_0 is the modified Bessel function of the order 0, which can be approximated by the exponent, the approximate right-hand side of (6). The relationship in (6) is very important for the ion funnel design, and more generally for any stacked ring ion guide since it provides a way to choose a correct ratio of the inner radius ρ to the spacing d, ensuring that the axial traps are sufficiently small compared to the maximum effective potential V^{*}_{ρ}. The condition can be expressed in a form of the following inequality:

$$2\pi\frac{\rho}{\delta}\exp\left(-\frac{2\rho}{\delta}\right)<<1 \tag{7}$$

The first ion funnel prototype used exit ring i.d.'s close to the spacing between electrodes, $2\rho \approx d$, or even smaller. Substituting $\rho/\delta \approx \pi/2$ into equation (4), we obtain $V_{\text{trap}} \approx 0.42 \quad V_{\rho}^{*}$, meaning that the axial effective potential wells are very pronounced and are nearly as intense as the maximum effective potential. Considering that the maximum potential (5) is reached at the maximum radial position, $r = \rho$, which corresponds to the ion loss, it is clear that the exit section worked to stop and trap ions rather than radially focus them.

The exponent in (6) leads to very fast decreasing of V_{trap} with increasing the ratio ρ/δ. Assuming $\rho = d$ we obtain $V_{\text{trap}}=0.037 \quad V_{\rho}^{*}$, a favorably low axial trapping potential consistent with inequality (7). This simple calculation explains why the second design (Shaffer et al., 1999), which used increased i.d.'s of the exit rings, demonstrated markedly improved performance.

The low *m/z* transmission range, related to the *m/z* instability, can be estimated using the adiabaticity parameter relationships. The adiabaticity condition implies that there is a negligible energy exchange between the macro and micro motion of ions, making it possible to apply the concept of effective potential (Gerlich, 1992). The condition is fulfilled when the amplitude of rf oscillations is small compared to the characteristic scale of rf field homogeneity. Approximately, low *m/z* ions acquire increased amplitudes of rf oscillations, approaching inter-electrode distance. The effective potential approach is inaccurate for such low *m/z* ions; computer simulations show that such ions cannot be efficiently confined by the rf field. As a result of this limit, the velocity of ions confined by the rf focusing is limited by $u_{max} = d \cdot f$, which determines the low *m/z* cutoff for low pressure conditions. A low *m/z* cutoff also arises from instability in the axial traps, which is likely to occur at the ion funnel exit where apertures become small compared to *d* (Tolmachev et al., 2000).

Another useful relationship provides evaluation of the ion current i_{max}, corresponding to the space charge limit on efficient ion transmission:

$$i_{\max}=\pi\varepsilon_0\tau\rho E_z\left(\frac{q}{m}\right)^2\frac{V_{rf}^2}{\omega^2\delta^3} \tag{8}$$

Here, ε_0 is the dielectric constant, τ is the ion velocity relaxation time (Tolmachev et al., 1997) related to the ion mobility K as follows: $\tau = m/z\ m_u\ K / e$, where e is elementary

charge and m_u is the atomic unit mass. Importantly, the ion current limit (8) is inversely proportional to the cubic power of the inter-electrode spacing $d = \pi\delta$. This is due to the effective focusing field, estimated as the derivative of the effective potential (4) by radius, being inversely proportional to d^3. It follows that the spacing minimization provides a way to greatly improve the ion funnel focusing efficiency.

The ion funnel rf frequency should be above a certain limit defined by adiabaticity requirements, which are more stringent for the smaller spacing *d*. The adiabaticity parameter is inversely proportional to the rf frequency squared (Gerlich 1992), thus higher frequencies can be used to offset the effect of reduced spacing; in practical terms, frequencies on the order of ~1 MHz are acceptable with the reduced spacing (Tolmachev et al., 2000). The spacing *d* should not be too small due to a limitation related to the z-velocity of ions, v_z: at low pressures, <~1 mTorr, where the mean free path is increased, ion velocities may exceed the limit $v_z < d \cdot f$; thus the lower pressure operation may require larger ring spacing and higher rf frequency (Tolmachev et al., 2000).

The reduction in electrode spacing of the current version of the ion funnel to d = 1 mm (Kim et al., 2000a) resulted in an increase in focusing power by ~30 times over previous designs, assuming the same rf voltage and frequency, considering the cubic power proportionality of the maximum effective rf focusing field on *d* (Tolmachev, 2000). This implied a capability of operation at increased pressures where the effective potential is suppressed (Tolmachev et al., 1997), and for 1 Torr pressure conditions it was estimated that the effective focusing is sufficient to overcome the drag force from gas flows up to sonic speeds (Tolmachev et al, 2000). The ring electrode proportions, and the distribution of ions inside the ion funnel can be seen in the simulation screen shot in Figure 5. The dependence of the ion transmission efficiency on the amplitude of the rf voltage V_{rf} showed threshold-like behavior for this design. As shown in Figure 6, the ion transmission was found to increase sharply at relatively low rf voltages (~20 $V_{p\text{-}p}$) and remain constant for a wide range of V_{rf}. The saturation level corresponded to an estimated transmission efficiency of ~100% for analyte ions. The behavior was consistent with the results of the computer model, also shown in Figure 6, which showed ion transmission reaching 100% efficiency for V_{rf} above a certain threshold voltage that was dependent on parameters including *m/z*, rf frequency, and pressure. For Figure 6, the ion current was measured after the ion funnel exit for pressure 1 Torr, input current 5 nA, frequency 0.7 MHz, axial dc field 16 V/cm. Simulations were carried out for the same conditions; the ion current was supposed to consist of equal amounts of 1+ and 2+ gramicidin ions.

An alternative ion funnel design supported by a simulation study has been reported by Jarrold and coworkers (Julian et al., 2005). An ion funnel electrode spacing of 5.6 mm was used, together with the smallest (exit) ring electrode i.d. of 7.9 mm. The funnel was typically operated at a pressure of ~220 mTorr, but it was also used successfully at pressures ranging from several Torr to ~50 mTorr. Ions with varying *m/z* between 75 and 3000 were passed through the funnel with no apparent discrimination. The study did not specify the ion transmission efficiency achieved, and no transmission profiles versus V_{rf} and *m/z* were reported. A simple method for simulating ion motion based on ion mobility (i.e., drift approximation) and diffusion was proposed, and a guideline for the boundary between the strong rf field and the field-free region was formulated, which is qualitatively consistent with the effective potential approximation. The increased spacing provided a number of practical advantages; as mentioned in Section II, the stacked ring ion guides operating at low pressures can use larger spacing to fulfill the condition $v_z < d \cdot f$ for increased axial ion velocities v_z.

Another direction of ion funnel development that has also benefited from modeling relates to extending the range of efficient operation to higher pressures (i.e., >30 Torr), which enables increased ion transmission efficiency at the MS inlet. In this case, the major challenge relates to the physics of ion motion at higher pressures, where the rf oscillations of ions are in phase with the rf field. The in-phase motion is due to the drift-like behavior, generally observed at a macroscopic scale in ion mobility experiments, where the ion velocity is proportional to the electric field strength. This is opposed to the vacuum case, where a phase shift is established between the rf field and the rf ion motion, which is required for the effective potential to be non-zero (Dehmelt, 1967; Gerlich, 1992; Ibrahim et al., 2006). A phase shift can still be developed at increased pressures if a sufficiently high rf frequency is used, $\omega\tau >> 1$ (Tolmachev et al., 1997). The theoretical and modeling results for the high pressure ion funnel were confirmed by experiments that demonstrated efficient operation at pressures up to 30 Torr using increased rf frequencies (Ibrahim et al., 2006).

C. Related RF Focusing Devices

Since the introduction of the ion funnel, a number of alternative devices have been developed to perform a related function, i.e., to improve ion transmission in the high pressure interface region of the mass spectrometer. For example, Shimadzu patented axially segmented multipoles having an inscribed radius that converged towards the exit (Inatsugu & Waki, 2002). A conical octopole ion guide described recently (Roach et al., 2008) also uses the converging geometry, but without axial segmentation, thus precluding the application of an axial dc field. Also, Thermo Fisher recently developed a stacked ring ion guide (Wouters et al., 2008) whose rf ring electrodes at the exit have a constant i.d. but are progressively spaced to effect ion focusing. In this section we describe these devices and contrast them with the ion funnel.

The segmented multipoles (Inatsugu & Waki, 2002) are somewhat similar to the ion funnel in their ability to produce rf ion focusing and a dc electric field to facilitate ion motion along the axis towards the exit of the ion guide. The converging geometry combines an increased ion acceptance area with the ability to create a tight ion beam at the exit, which is again similar to the ion funnel. A potential disadvantage of the multipolar, rather than the stacked ring geometry, however, is that the rf focusing at the first entrance segment is significantly reduced, due to an increased distance d between rods having opposite rf phases. For example, consider a segmented multipole whose inscribed radius decreases along the axis by a factor of 10, similar to commonly used ion funnel configurations that have a 25 mm entrance i.d. and a 2.5 mm exit electrode i.d. (Page et al., 2007). The effective potential is proportional to the rf electric field intensity squared, eq. (1), thus a 10-fold increased spacing d converts into a 100-fold reduced effective potential. This can greatly limit the ability to compensate for the drag forces from intense gas flows typically occurring at the entrance of the ion guide in higher-pressure regions. The coulombic expansion of the ion beam will contribute to the radial ion losses at the entrance, due to the reduced effective potential. According to the theoretical evaluation of the ion funnel (Tolmachev et al., 2000), the radial effective field, defined as the derivative of the effective potential by radius, is responsible for counterbalancing the gas flow drag force and the coulombic ion expansion. Approximately, the effective field is inversely proportional to the cubic power of distance d:

$$E^* \sim 1/d^3 \tag{9}$$

The cubic dependence results from the effective potential being proportional to the rf field intensity squared (Gerlich, 1992); the additional factor ~d arises when the derivative of the effective potential is taken to obtain the effective focusing field. A factor of 10 convergence thus results in 1000 times weaker entrance rf focusing defined by the effective field if the

multipolar geometry is used. The issue cannot be solved by simply increasing rf voltage, since this will increase low-*m/z* instability at the exit. Even with an axially adjusted rf voltage profile, the requirements for rf amplitude at the entrance would be much greater than for an ion funnel that uses a small, non-variable spacing d = 1 mm (Tolmachev et al., 2000). Thus, the design suffers from a finite size of the ion entrance area. Additionally, the *m/z* transmission range in each segment will vary, thus limiting the overall *m/z* transmission.

Tapered multipoles (Roach et al., 2008) that resemble standard rf multipole ion guides but are arranged with a conical taper decreasing toward the exit have also been explored. These are similar in concept to the segmented multipoles described above, but lack the ability to apply a dc gradient or to apply stronger rf at the entrance to compensate for the weaker focusing field, and as such are expected to have limited transmission efficiency. In addition, as for the above design, the *m/z* transmission characteristics will vary with axial location, limiting the *m/z* transmission range.

A variation on the ion funnel that was recently described by researchers at Thermo Fisher is the progressively spaced stacked ring ion guide, which has demonstrated improved ion transmission relative to the standard skimmer interface of a triple quadrupole mass spectrometer (Wouters et al., 2008). The prototype comprised a small number of ring electrodes (18), similar to the original ion funnel (Shaffer et al., 1997), and incorporated two adjacent stacked ring ion guide sections, with the first section having a larger ring diameter than the second. In addition to decreasing the diameter of the ring electrodes part way through the device, the increased electrode spacing toward the exit produces an increasing rf electric field that further focuses ions, even with constant ring electrode i.d. The design uses no dc potential gradient to drive ion transmission, relying solely on the flow of gas expanding from the heated inlet capillary.

Unlike modern ion funnels, which capture and transmit ions with ~100% efficiency over a broad *m/z* range using fixed rf voltage and frequency (Tolmachev et al., 2000), all of the above exhibit a strong dependence of the *m/z* range transmitted on rf. In the Thermo design, this made it necessary to modulate the rf amplitude (by a factor of 30) in concert with the scanning of the quadrupole mass analyzer to transmit ions over a broad *m/z* range. This linked scanning approach, similar to that described for an early ion funnel prototype (Shaffer et al., 1999), is most appropriate only with scanning/mass filter-based analyzers, and would be ineffective with ion traps, FTICR, TOF, etc. It appears that, as with early ion funnel prototypes (Shaffer et al., 1997), the device suffers from severe axial wells in the rf effective potential, which form in part because of the large ratio of the electrode spacing d to the ring inscribed radius ρ (i.e., $d/\rho \sim 2$). However, unlike the ion funnel, where such wells can be minimized by decreasing d/ρ, a strong axial field is an unavoidable consequence of the progressive spacing. Consider conventional stacked ring ion guides and ion funnels, in which the constant, non-variable inter-electrode spacing creates a “local symmetry” in the axial direction. Ring electrodes with alternating phases of rf compensate each other, enabling a strong radial effective potential with a minimal axial component. An essentially field-free region begins when the distance from an electrode is ~60% of the distance between the electrodes (Julian et al., 2005). With variable spacing this symmetry is disrupted, contributing to increased axial rf electric fields. When the ratio d/ρ becomes large, > 1, the off-axis field becomes comparable to the on-axis field in between neighboring electrodes, producing a weak radial focusing combined with an increased axial barrier. The axial wells can trap ions of a certain *m/z* range, creating the defocusing radial coulombic electric field. Low *m/z* ions acquire increased amplitudes of rf oscillation and can be either fragmented or ejected. If not ejected, experimental artifacts can become evident in the mass spectra (e.g., as multiply charged ions dissociate to yield higher *m/z* products).

All rf ion guide types used currently in mass spectrometry avoid the creation of intense rf fields around the axis. Ideally, the rf focusing relies on zero rf fields at the axis, combined with intense rf fields at off-axis radial positions. An example of such a configuration is the rf multipole ion guide, where rf field intensity approaches zero at the axis, due to symmetry. Reducing rf field intensity along the axis is critical for operation at pressures >1 mTorr to avoid collisional activation of ions. With the progressively spaced stacked ring ion guide, an increased rf voltage would be required to offset relatively large interelectrode spacing, resulting in further increased intensities of rf fields around the axis, which can result in collisional activation of ions.

The authors observed a five-fold sensitivity improvement over the standard skimmer interface (Wouters et al., 2008), which is somewhat smaller than the order-of-magnitude gains provided by the ion funnel when used for similar comparisons (Page et al., 2007). Also, it is not clear how much of the improvement was due to the stepwise decrease in ring electrode i.d. along the axis, and what portion was derived from the progressive spacing. Our simulations of such devices using increased d/ρ ratios showed the transmission optimum depends on conditions that are difficult to control, including gas flow velocity and ion current variations. Sample simulation results in Figure 7 show the ion transmission profiles simulated for a test configuration of the progressively spaced stacked ring ion guide. For all conditions evaluated, the ion transmission was below 30% and the transmission optimum was dependent on m/z, ion current, and gas flow velocity. In addition, the model showed more stable operation with respect to the gas flow velocity and the ion current when an axial dc gradient was applied.

IV APPLICATIONS

A. Increased transmission efficiency from elevated pressure ion sources

Having established the ability of the ion funnel to effectively transmit ions between the first and second differentially pumped vacuum stages, researchers sought to further leverage the ion funnel to reduce ion losses through the atmospheric pressure interface. Such a design, capable of high transmission efficiency from the atmospheric pressure ion source to high vacuum would enable unprecedented sensitivity and also improved quantitation, as m/z-dependent transmission biases (Lin & Sunner, 1994) would be eliminated. Several approaches for using the ion funnel to improve the transmission of ions from the ESI source into the mass spectrometer are shown in Figure 8.

Initial efforts to increase transmission through the atmospheric pressure interface by simply increasing the diameter of the heated capillary inlet and adding pumping speed to the first differentially pumped stage (Kim et al., 2000a) were unsuccessful due to less efficient desolvation of the electrosprayed droplets. Also, with increasing inlet diameters the gas flow transitions from laminar to turbulent, leading to large ion losses. To preserve the desolvation afforded by a standard inlet while increasing conductance, an interface having multiple, narrow-bore (400–500 μm i.d.) heated inlet capillaries was evaluated (Kim et al., 2000b). The use of multi-capillary inlets was made possible by the large entrance aperture of the ion funnel. A skimmer interface, for example, would be unable to efficiently sample ions entering the first vacuum stage significantly off-axis. The multi-capillary inlet led to dramatic sensitivity gains; however, the increased conductance required the use of two high-speed pumps (Figure 8B) to maintain the appropriate downstream vacuum pressures.

To eliminate the need for high speed pumps and make possible the routine use of multi-capillary inlets, the working pressure of the ion funnel was increased to ~30 Torr (Ibrahim et al., 2006). The previous pressure limitation on the ion funnel was due to the need for greater rf frequency and amplitude at elevated pressures to compensate for the increased collisional

frequency of ions with background gas at elevated pressures and the lower effective confining field (see Section IIIB). The large electrical capacitance of the ion funnel precluded the application of greater rf; excess metal was therefore removed from the electrodes, lowering the capacitance approximately four-fold. With the reduced capacitance, the ion funnel operated with a 1.74 MHz rf and up to 170 V_{p-p}, and demonstrated ion transmission efficiencies at pressures as high as 30 Torr that were similar to a standard ion funnel designed for 2 Torr. The reduced pumping requirements enabled by the higher pressure ion funnel were made possible by an additional pumping stage, as depicted in Figure 8C. Here, the additional stage was a second ion funnel immediately behind the higher pressure ion funnel. This ion funnel chamber was operated at 1.3 Torr and used a standard rf frequency and amplitude (560 kHz and 70 V_{p-p}). This arrangement demonstrated how multiple ion funnels can be coupled in series with minimal ion losses to customize the inlet conductance requirements, while maintaining the pressures in the downstream ion optics of the instrument using standard rough pumps. A five-fold sensitivity enhancement was observed for a single emitter used in conjunction with an 18 heated capillary inlet design compared to when a single inlet was used.

B. Improving ionization efficiency with multi-emitter ESI sources

The multi-capillary inlet/ion funnel interfaces described above have also enabled new techniques for improving ionization efficiency, which is greatly enhanced when the electrospray is operated at low nL/min flow rates (Gale & Smith, 1993; Wilm & Mann, 1994). The higher flow rates from typical capillary LC separations preclude the use of nano-ESI without wasteful post-column flow splitting (Fuh & Hsieh, 1999; Andrews et al., 2004), and operation of LC at nano-ESI-compatible flow rates (<100 nL/min) severely decreases the sample loading capacity and can lead to reduced system robustness (Smith et al., 2004). As an alternative, the multiple inlets developed to increase conductance into the first vacuum stage also make possible the efficient sampling from multiple electrospray emitters, effectively reducing the flow at each emitter and producing multiple, highly efficient electrosprays. Although multiplexed electrosprays had been demonstrated previously (Rulison & Flagan, 1993; Almekinders & Jones, 1999), the first multi-emitter designed specifically for increased MS sensitivity used an ion funnel interface with a multi-capillary inlet (Tang et al., 2001). The microchip-based array of 9 emitters was able to produce multiple, stable electrosprays at flows as low as 300 nL/min at each emitter. Recent advances have increased the number of individual emitters and reduced the flow rates accessible to each emitter in the array (Kelly et al., 2007; Kelly et al., 2008b). A linearly arranged 19 electrospray emitter array coupled to a 19 capillary inlet and an ion funnel operated at 18 Torr provided a ~9-fold MS sensitivity enhancement compared to a single electrospray emitter/single inlet ion funnel interface (Kelly et al., 2007). The emitter array was comprised of fused silica capillaries that were tapered using a chemical etching technique (Kelly et al., 2006) to provide high aspect ratio, externally tapered emitters, each capable of operating at flows as low as 20 nL/min. A 19 capillary (each 400 μm i.d.) heated inlet was used to match each emitter in the array with an individual inlet to the ion funnel. The emitter array and ion funnel interface were tested by infusing and analyzing a bovine serum albumin (BSA) tryptic digest solution with a single emitter and the multi-emitter array. A broad range of sensitivity improvements for the tryptic peptides was observed, from 2.4- to 12.4-fold, and the differences were attributed to variable reductions in ionization suppression when the multi-emitter array was used; individual electrosprays were operated at ~50 nL/min. Reduced ion suppression was further verified by infusing a test mixture containing a peptide and an oligosaccharide over a range of flows with an individual emitter and the emitter array. At each common flow rate, the oligosaccharide, which is typically highly suppressed due to its low surface activity (Schmidt et al., 2001), exhibited a stronger

relative intensity when the array was used in place of the individual emitter, as the smaller droplets ensured more complete desolvation.

More recently, the 19 emitter array and ion funnel interface were coupled to an HPLC separation operating at 2 μL/min to analyze human plasma tryptic digest samples (Kelly et al., 2008b). Standard proteins not found in human blood plasma were spiked into the samples prior to digestion and analyzed by HPLC coupled to a TOF MS. Compared with a single emitter/single inlet configuration, the multi-emitter array provided an 11-fold average increase in MS sensitivity for the spiked peptides, and the LC peak *S/N* increased ~7-fold. In addition, the low dead volume of the emitter array preserved chromatographic peak shapes, such that the separation efficiency was retained. In this work, direct infusion experiments compared the multi-emitter/multi inlet interface to the standard skimmer interface of the unmodified instrument using a mixture of standard peptides. The cumulative sensitivity gains relative to a standard skimmer interface for a peptide mixture resulting from the combination of the multi-emitters, a multi-capillary inlet and a tandem ion funnel interface (Ibrahim et al., 2006) are shown in Figure 9. The capillary-based emitter arrays have since been reconfigured to a circular arrangement to improve the inter-emitter electric field uniformity, which can otherwise be disrupted as a result of inhomogeneous electrical shielding caused by the closely spaced emitters (Kelly et al., 2008a).

C. Subambient pressure electrospray

ESI emitter arrays and multi-capillary inlets increase MS sensitivity when coupled with an ion funnel interface; however, significant losses can still occur during transmission into the mass spectrometer (Kelly et al., 2008a). Recently, ion funnel technology has enabled the electrospray to be operated inside the first vacuum region of the mass spectrometer (Page et al., 2008a), completely eliminating the transmission losses that normally occur at the inlet. The new subambient pressure ionization with nanoelectrospray (SPIN) source, depicted in Figure 8D, used small (5 to 10 μm i.d.) chemically etched emitters positioned at the inlet of an ion funnel, where both the electrospray and ion transmission occurred at 30 Torr. The pressure was low enough to ensure effective ion funnel operation, but sufficiently high to provide adequate droplet desolvation while avoiding electrical discharge. Initial characterization of the SPIN source showed stable electrosprays with a variety of LC-compatible solvents (i.e., water, methanol, and acetonitrile) at pressures ranging from 760 to 25 Torr. Electrospray current profiles were obtained using an array of charge collectors and showed that the electrospray current remained unchanged through the range of pressures, while the plume became narrower at lower pressures due to increased droplet/ion mobilities (Gamero-Castaño et al., 1998). Using two different solutions, a ~6-fold increase in sensitivity was demonstrated when the SPIN source replaced a heated capillary inlet interface, indicating that sample losses that normally occur through an inlet were eliminated, while the ionization efficiency was largely preserved. In subsequent experiments, the SPIN source was used with LC-MS to analyze a protein digest sample (Page et al., 2008b). Compared to a standard inlet, the SPIN source produced a 5–12-fold increase in sensitivity for detected peptides, again demonstrating increased detector response through reduced ion losses and also showing stable operation at 30 Torr for a range of solvent compositions provided by gradient elution LC. The SPIN source promises to be an enabling technology for additional novel ESI source designs.

D. Ion Mobility Spectrometry and Ion Trapping

Ion funnel technology has benefitted IMS instrumentation in ways that extend far beyond improved ion transmission through the ESI interface. As we describe in this section, the ion funnel has also been incorporated at locations along the IMS drift tube as well as at the distal end to counteract diffusion and make possible high sensitivity, high resolution IMS-MS.

Also, the ion funnel has been adapted to trap, store and release ions from continuous beam ESI sources for maximizing the duty cycle with inherently pulsed IMS operation. Ion funnel traps (IFTs) are of broader applicability than for IMS alone, but because much of the IFT development has been applied to improving IMS duty cycle, we present the applications related to both ion trapping and IMS together in this section.

The first implementation of the ion funnel with an IMS instrument, reported by Bowers and coworkers (Wyttenbach et al., 2001), was used to trap ions in between injections into the ion mobility drift cell, as well as to effectively transmit ions through the ESI interface. The drift cell operated at much lower pressures (0.02 Torr) and with a far shorter drift cell (4.5 cm) than subsequent designs that incorporated ion funnels, and as such, was capable of sub-millisecond separations having injection pulse rates of 1–10 kHz. With such rapid injections involving relatively small ion populations, the potential applied to the penultimate ion funnel electrode could be modulated to accumulate ions in between pulses with a trapping efficiency of nearly 100%. The ion funnel itself was based on the original design of Shaffer, et al. (1998), but following the tapered section, two straight sections were incorporated to help mitigate the transmission biases of the Shaffer design. The initial characterization of the ESI-IMS instrumentation used a quadrupole mass analyzer to study the thermodynamics of peptide hydration, perform structural analyses of biomolecules, and to measure reaction rate coefficients. The instrument has enjoyed continued use for numerous studies; for examples, see (Gidden et al., 2004; Gidden et al., 2005; Baker et al., 2006; Liu et al., 2006; Baker & Bowers, 2007).

The use of IMS as an orthogonal separation dimension in between LC and MS is of particular interest for high throughput analyses of complex samples, such as global proteomics applications. For the required high resolution separations, longer drift cells operated at higher pressures are necessary, and the time scale of the IMS separation (~10–100 ms) is such that multiple mass spectra (e.g, from TOF MS) can be collected across each IMS peak. Despite the enormous potential of a high resolution LC-IMS-TOF MS platform, a major challenge has been the low sensitivity resulting from ion losses before and following the drift tube. By incorporating ion funnels at both the entrance and exit of the drift tube, the design of Tang et al. (2005) provided a major advance in increasing the sensitivity of ESI-IMS-TOF MS. The IMS drift tube was operated at 4 Torr, and the ion funnel at the ESI interface served to both focus and store ions to reduce losses in between injections. As shown in Figure 10, this ion funnel had an hourglass shape, enabling a conductance limit at the narrowest ring electrode and increased storage volume inside the flared portion that followed. A high transmission grid after the final ion funnel electrode served as an ion gate, preventing the passage of ions in between injection events. Without this ion storage, the submillisecond injections would afford a duty cycle on the order of just ~1%, making the efficient use of ions via trapping vital for high sensitivity measurements.

Perhaps the most significant aspect of the Tang et al. design was the incorporation of a second ion funnel where the end of the IMS drift tube interfaced with the TOF mass spectrometer. The differential pumping requirements between the two chambers dictate a small, conductance limiting aperture. Without the ability to focus ions at the end of a long drift tube, the diffusional and in some cases space-charge-driven expansion of the ion packet result in severe ion losses. The ion funnel at the drift tube exit had a 51 mm acceptance aperture, which ensured essentially lossless transmission to the TOF. The efficient transmission was verified by interfacing the ESI source to the TOF directly, i.e., without the 147 cm long drift tube used for comparison, and observing similar ion intensities. Sensitivity was also not significantly affected by increasing the length of the drift tube from 105 to 210 cm, provided a potential of at least 3.5–4 kV was applied across the drift tube. A resolution of ~120 was achieved for singly charged peptides, which was close to the theoretical limit

once the ion injection pulse and the TOF spectrum acquisition frequency were accounted for, indicating that the ion funnel at the exit of the drift tube did not measurably degrade IMS resolution. A 0.6 s analysis (10 averaged scans) showed a high quality arrival time distribution for a 10 μM peptide solution, which verified the improved sensitivity over previous designs.

In a subsequent study, Baker et al. (2007) replaced the ion funnels at the entrance and exit of an 88 cm drift cell with low-capacitance ion funnels (Ibrahim et al., 2006) that were capable of efficient operation at pressures as high as 12 Torr, rather than a maximum of 4 Torr for the previous design (Tang et al., 2005). Ignoring sources of broadening outside of the drift cell, peak resolution is proportional to the voltage drop through the cell (Asbury & Hill, 2000). However, above a certain *E/N*, where *E* is the electric field and *N* is the number density of the bath gas, ion mobilities become dependent on *E/N*, and measured arrival time distributions are distorted. By increasing the operating pressure of the drift cell, higher electric fields become accessible without the negative effects associated with exceeding the low-field limit. The reduced capacitance allowed for increased rf frequencies, and a non-tapered section was added to the terminus of the “hourglass” ion funnel to further increase trapping capacity. Operation at 12 Torr enabled the resolving power of the IMS separation to increase to ~80, compared with ~50 at 4 Torr, without a significant loss of sensitivity.

The utility of the ion funnel for ion mobility studies was extended by Clemmer and coworkers (Koeniger et al., 2006), who developed a highly flexible instrument capable of several operational modes. Key to the design was a drift tube divided into two regions. An hourglass-shaped ion funnel, essentially the same as that of Tang et al. (2005), was placed at the beginning of the drift tube and was used for storing and pulsing ions into the drift tube as before. Two additional ion funnels were placed at the center and end of the drift tube, respectively. The final ion funnel was used for efficient transmission into the TOF and could also be used to induce fragmentation if desired. The center ion funnel, combined with an ion activation region and a grid used for gating, could be used to select ions of a certain mobility range from the first stage of the drift tube, collisionally activate or fragment those ions, and separate the resulting conformers or fragments according to mobility in the latter portion of the drift tube prior to MS. This was notably the first IMS—IMS analogue to MS—MS.

An additional benefit to incorporating ion funnels along the drift tube is that the separation length could be made arbitrarily long without incurring large ion losses, as the broadening ion packet could be refocused multiple times without diminishing resolution. An example of such a design was also described by Clemmer and coworkers (Merenbloom et al., 2006). The 290-cm-long drift tube assembly had ion funnels at the beginning and end of the drift tube, in addition to two ion funnels along the length. These additional ion funnels divided the drift tube into three distinct regions and made possible high resolution IMS—IMS—IMS/MS separations of proteins and peptides, and were capable of resolving many features that could not be identified by MS alone.

While IMS clearly benefits from the ability of the ion funnel to trap and store ions for rapid injection, other instruments can also take advantage of ion trapping. TOF MS is an inherently pulsed technique, with a limited duty cycle when used in conjunction with a continuous ESI source, and Ibrahim et al. (2007) have explored an IFT for improving TOF performance. The ion funnel trap had a unique geometry, as shown in Figure 11, that resembled the hourglass ion funnel described by Baker et al. (2007), but included a final section that refocused the ions released from the trap to a conductance limiting orifice. High-transmission grids defined the entrance and exit of the fixed-width trapping section, and were respectively used as gates to control the ion population in the trap and to release ions into the TOF. The dc gradient in the trapping region was adjusted independently from the

rest of the IFT, and was found to provide optimum performance with a shallow gradient (4 V/cm), alleviating space-charge-related ion losses that occurred with steeper gradients as a result of a more compressed ion cloud. The linear dynamic range for the trap extended to ~10^7 charges, and the intensity of the released ion packets increased linearly with accumulation times up to 20 ms for a model analyte, regardless of concentration. Importantly, for solutions containing 10 nM peptides, the maximum sensitivity gains for the ion trapping TOF relative to continuous mode ranged from 13–20-fold. Improvements in *S/N* were even more pronounced, up to 35-fold, and were largely attributed to improvements in desolvation and declustering that occurred due to a gentle rf heating for longer periods during trapping. The improved *S/N* enabled the detection of neurotensin at a concentration of just 100 pM, while the peak was buried in the chemical noise for continuous mode. Because extraction from the trap at 1 Torr was mobility-based, sufficiently fast extraction times could preferentially select multiply charged species while almost completely rejecting singly charged ions. This could be used to further improve *S/N* for chemical noise limited analyses of multiply charged species including proteins and peptides, as such noise-related species are generally singly charged (Kast et al., 2003).

The IFT has since been used to implement automated gain control (AGC) with LC-ESI-TOF MS analyses (Ibrahim et al., 2008). While it is vitally important to transmit ions from the ESI source with high efficiency, particularly for the detection of trace species, excessive ion currents can also degrade TOF resolving power due to detector saturation and an increased distribution of radial velocities in the extraction region. When coupled with HPLC analyses, the IFT was used to attenuate the currents entering the TOF when intense peaks were eluted from the LC such that high resolving power was maintained throughout the analysis, and also to maximize the transmission of trace species. For the smallest samples analyzed (500 ng), the approach provided a dramatic five-fold increase in the number of unique peptides identified from a *S. Oneidensis* global tryptic digest compared to when trapping and AGC were not used (i.e., continuous mode).

Clowers et al. (2008) recently refined the IFT described above (Ibrahim et al., 2007) and evaluated its performance for IMS ion introduction. The principal hardware modification was the addition of a second grid at the exit of the trapping region. This created a more uniform radial potential distribution during accumulation, allowing ions to accumulate closer to the exit grids. As a result, the ion storage capacity of the trap increased by ~50%, and fast ejection times were maintained at pressures as high as 4 Torr. When used for IMS with a charge collector for detection, the intensity of the detected peptide peak increased ~7-fold for a 400 μs injection relative to the currents measured when ions were introduced continuously. The overall accumulation efficiency was evaluated as a function of accumulation time for different pressures (2 and 4 Torr) and peptide concentrations. The efficiency varied from ~10% to nearly 100% depending on the conditions, and was most adversely affected by longer storage times. Still, an ion utilization efficiency of 10% for an 80 ms accumulation represents a marked improvement over conventional gating approaches. The ion funnel trap was also used for IMS-TOF MS experiments, and the gains observed using the charge collector were verified. Evaluation of the percent coverage of a BSA tryptic digest as a function of accumulation time showed a maximum at 10 ms; longer accumulations reduced coverage by as much as ~20%. This observation was attributed to ion discrimination in the trap that occurred once the charge capacity was exceeded.

E. Calibrant Introduction for High Mass Measurement Accuracy Analyses

As the demand for ultra-high mass measurement accuracy (MMA) has grown, particularly with the spread of high-resolution instrumentation and the application to complex biological samples (Liu et al., 2007), the need for internal calibration methods has increased. Introduction of a calibrant with the analyte through the same electrospray source can

negatively impact an analysis due to ion suppression and added space charge in the mass analyzer, making independently controlled, separate electrospray sources more attractive. To avoid the potential reduction in duty cycle and the moving parts associated with mechanically switching between analyte and calibrant emitters (Hannis & Muddiman, 2000; Flora et al., 2001), a dual-channel ion funnel was developed (Tang et al., 2002). The front section of the ion funnel contained a series of electrodes, each having two rings, such that two distinct channels were formed. The channels were aligned with individual heated capillary inlets; one was used for the standard transmission of analyte ions, while the second channel was used for calibrant. The voltage applied to the jet disrupter electrode in the calibrant channel could be modulated rapidly to either pass ions or block their passage, and such modulations were shown not to affect the transmission of ions through the analyte channel. The separate channels merged prior to the exit of the ion funnel such that two separate ion streams were focused together and transmitted to high vacuum.

F. Tuning Ion Transmission

The ability to tune the transmission characteristics in the ESI source can improve instrument performance in ion trapping instruments where unwanted lower *m/z* species can occupy "charge space" in the trap, degrading dynamic range and sensitivity (Shwartz et al., 1996). The fundamental mechanisms of ion transmission and the multiple dc and rf elements of the ion funnel enabled ion beam manipulations that were not possible with standard skimmer interface designs. As in Section III, early ion funnel interfaces exhibited *m/z* discrimination and narrow transmission windows that were problematic and not well understood (Shaffer et al., 1997; Shaffer et al., 1998). However, as the technology progressed, the ion funnel provided a much broader transmission window with minimal discrimination and the ability to tune the transmission in a controlled fashion.

Manipulation of the rf frequency and the axial dc field was shown to easily control the lower *m/z* limit of the ion funnel (Page et al., 2006). This was demonstrated by varying the rf frequency from 700 to 100 kHz, which resulted in a low *m/z* cut-off in the ion funnel that increased progressively from ~100–1000 *m/z*. The dc gradient was also changed from 9 to 29 V/cm, and steeper dc gradients were found to increase the lower *m/z* cutoff. The experimental results were used with a theoretical model to develop mathematical relationships for both the low and high *m/z* cutoffs of an ion funnel. Filtering of lower *m/z* ions was also accomplished by creating a dc potential barrier at the exit of the ion funnel and using the mobility of the ions to selectively pass them to the mass analyzer (Page et al., 2005b). Here, the potential on the final ion funnel electrode, which served as the conductance limit, was varied over a range of 10 V and provided effective, linear filtering of background species from 0 to 500 *m/z*. The filter was tested with an LC analysis of a BSA tryptic digest solution. The ion current exiting the ion funnel was recorded with and without the low *m/z* filter, and showed that 40–70% of the total ion current was from unwanted "background" species. The jet disrupter electrode was also used as an "ion valve" to regulate the intensity of the ion beam to prohibit the overfilling of an ICR cellin another implementation of AGC (Page et al., 2005a). The voltage applied to the jet disrupter was automatically adjusted within a 30 V range to vary the transmission efficiency of the ion funnel. More intense ion beams, from the LC elution of more concentrated species, initiated a calculated reduction in transmission efficiency to maintain a desired ion population in the ICR cell, improving MMA and data quality.

G. Other Novel Applications

The Tureček group developed an ion funnel interface for neutralization—reionization studies of electrosprayed ions for mechanistic studies (Seymour et al., 2003). To compensate for the low yields of the various reactions, in addition to other losses in the instrument, it

was important that the source provide efficient ion transmission. The ion funnel that was employed was modeled after the initial prototype developed by Shaffer, et al. (1997; 1998). This design has been shown to have a limited *m/z* transmission window, but for the intended application, the ion funnel could be tuned for maximum transmission of the individual species being studied. The interface proved capable of transmitting 1–2 nA of current and has been used successfully for a number of investigations (Chen et al., 2005; Yao et al., 2005; Chen & Tureček, 2006; Jones et al., 2007; Yao et al., 2007). The same group has also used an electrospray—ion funnel interface for immobilizing biomolecules on plasma-modified surfaces (Kitching et al., 2003), and have since adapted the platform for soft landing of biomolecules, including multiply charged protein ions (Volny et al., 2005;Volny & Tureček, 2006; Volny et al., 2007) and preparative MS separations with subsequent soft-landing recovery of parent molecules from electrosprayed mixtures (Mayer et al., 2005). In all cases, throughput was critical, and the ion funnel served to efficiently transfer ions into high-vacuum.

The Armentrout group has recently incorporated an ion funnel into the electrospray interface of a guided ion beam mass spectrometer (Moision & Armentrout, 2007). The intended application of performing thermochemical investigations using threshold collision-induced dissociation placed stringent requirements on the ion source. Besides providing a stable, intense ion beam, the source needed to produce ions having well defined kinetic energy distributions and internal energies described by a room-temperature Maxwell-Boltzmann distribution. The 88-plate jet disrupter-equipped ion funnel was based largely on previously published designs (Kim et al., 2001; Tang et al., 2002), but with a single wire soldered to each of the plates and connected to a custom-built circuit board through which both rf and dc potentials were applied. The ion funnel operated at ~0.01 Torr, considerably lower than the pressures employed in most designs. In initial experiments, the authors found that rf heating in the ion funnel produced ions that had internal energies exceeding their thermal temperatures, and that to avoid such heating it was necessary to operate at significantly lower rf potentials. Unfortunately, the reduced potentials were insufficient for ion focusing and the signal diminished. As a solution, the ion funnel was operated to produce maximum signal, but an rf-only hexapole that spanned two differentially pumped chambers was inserted after the ion funnel to thermalize the focused ions. The authors also tested a design in which the ion funnel was removed and the hexapole alone was used, but found that droplets and solvent clusters from the electrospray rapidly fouled the hexapole rods and degraded performance. Thus, in this design, the jet disrupter and ion funnel primarily served to remove unwanted contaminants while preserving sensitivity, which enabled stable, robust operation of the instrument for extended periods. The same group has since used the ESI-ion funnel interface with slight modifications to investigate the bond energies of $Ca^{2+}(H_2O)_x$ complexes (Carl et al., 2007).

Researchers have also used ion funnels for atomic physics applications. Specifically, ion funnel designs have been used to cool intense, low-energy radioactive ion beams (Varentsov & Habs, 2002; Heinz et al., 2004; Block et al., 2006; Neumayr et al., 2006a; Neumayr et al., 2006b; Block et al., 2007; Eliseev et al., 2007). In one proof-of-concept experiment (Heinz et al., 2004), a He buffer gas was used to cool and transfer 20 nA beams of ^{129}Xe with 65% efficiency using a 450-mm-long ion funnel that had a maximum i.d. of 60 mm. The ion funnel has been successfully implemented into a Penning-trap mass spectrometer that measures rare isotopes from fusion-evaporation reactions (Neumayr et al., 2006a; Block et al., 2007). Such diverse applications further demonstrate the broad potential of the ion funnel concept.

V CONCLUSIONS

Over the past decade the ion funnel has proven to be effective for improving the sensitivity of ESI-MS and highly versatile, as evidenced by the diverse applications outside of the field of ESI-MS. While much of the ion funnel development to date has stemmed from our laboratory, research by independent groups is increasing. Admittedly, the resource intensive nature of the state-of-the-art designs, requiring significant costs for machining and supporting electronics, as well as some technical expertise may in some cases deter otherwise interested researchers. The broader spread of the ion funnel will therefore likely happen as manufacturers of MS instrumentation continue to adopt the technology, increasing accessibility and allowing economies of scale to sharply reduce the associated costs. Even as commercialization spreads, we expect that innovative, independent researchers will continue to make refinements and find novel applications for the foreseeable future.

Acknowledgments

Portions of this research were supported by the U.S. Department of Energy (DOE) Office of Biological and Environmental Research, the NIH National Center for Research Resources (RR018522), the NIH National Cancer Institute, and the National Institute of Allergy and Infectious Diseases NIH/DHHS through interagency agreement Y1-AI-4894-01NIH. This research was performed in the Environmental Molecular Sciences Laboratory, a U.S. DOE national scientific user facility located at the Pacific Northwest National Laboratory (PNNL) in Richland, Washington. PNNL is a multiprogram national laboratory operated by Battelle for the DOE under Contract No. DE-AC05-76RLO 1830.

REFERENCES

Almekinders JC, Jones C. Multiple jet electrohydrodynamic spraying and applications. J. Aerosol Sci. 1999; 30:969–971.

Andrews CL, Yu C-P, Yang E, Vouros P. Improved liquid chromatography—mass spectrometry performance in quantitative analysis using a nanosplitter interface. J. Chromatogr. A. 2004; 1053:151–159. [PubMed: 15543981]

Asbury GR, Hill HH. Evaluation of ultrahigh resolution ion mobility spectrometry as an analytical separation device in chromatographic terms. J. Microcolumn Sep. 2000; 12:172–178.

Baker ES, Hong JW, Gaylord BS, Bazan GC, Bowers MT. PNA/dsDNA complexes: Site specific binding and dsDNA biosensor applications. J. Am. Chem. Soc. 2006; 128:8484–8492. [PubMed: 16802814]

Baker ES, Bowers MT. B-DNA helix stability in a solvent-free environment. J. Am. Soc. Mass Spectrom. 2007; 18:1188–1195. [PubMed: 17434745]

Baker ES, Clowers BH, Li F, Tang K, Tolmachev AV, Prior DC, Belov ME, Smith RD. Ion mobility spectrometry—mass spectrometry performance using electrodynamic ion funnels and elevated drift gas pressures. J. Am. Soc. Mass Spectrom. 2007; 18:1176–1187. [PubMed: 17512752]

Belov ME, Gorshkov MV, Udseth HR, Anderson GA, Smith RD. Zeptomole-sensitivity electrospray ionization—fourier transform ion cyclotron resonance mass spectrometry of proteins. Anal. Chem. 2000a; 72:2271–2279. [PubMed: 10845374]

Belov ME, Gorshkov MV, Udseth HR, Anderson GA, Tolmachev AV, Prior DC, Harkewicz R, Smith RD. Initial implementation of an electrodynamic ion funnel with FTICR mass spectrometry. J. Am. Soc. Mass Spectrom. 2000b; 11:19–23. [PubMed: 10631660]

Block M, Ackermann D, Blaum K, Chaudhuri A, Di Z, Eliseev S, Ferrer R, Habs D, Herfurth F, Heßberger FP, Hofmann S, Kluge H-J, Maero G, Martín A, Marx G, Mazzocco M, Mukherjee M, Neumayr JB, Plaß WR, Quint W, Rahaman S, Rauth C, Rodríguez D, Scheidenberger C, Schweikhard L, Thirolf PG, Vorobjev G, Weber C. Mass measurements in the endpoint region of the rp-process at SHIPTRAP. Hyperfine Interact. 2006; 173:133–142.

Block M, Ackermann D, Blaum K, Chaudhuri A, Di Z, Eliseev S, Ferrer R, Habs D, Herfurth F, Heßberger FP, Hofmann S, Kluge H-J, Maero G, Martín A, Marx G, Mazzocco M, Mukherjee M,

Neumayr JB, Plaß WR, Quint W, Rahaman S, Rauth C, Rodríguez D, Scheidenberger C, Schweikhard L, Thirolf PG, Vorobjev G, Weber C. Towards direct mass measurements of nobelium at SHIPTRAP. Eur. Phys. J. D. 2007; 45:39–45.

Carl DR, Moision RM, Armentrout PB. Binding energies for the inner hydration shells of Ca^{2+}: An experimental and theoretical investigation of $Ca^{2+}(H2O)_x$ complexes (x=5–9). Int. J. Mass Spectrom. 2007; 265:308–325.

Chen X, Syrstad EA, Nguyen MT, Gerbaux P, Tureček F. Adenine radicals in the gas phase: an experimental and computational study of hydrogen atom adducts to adenine. J. Phys. Chem. A. 2005; 109:8121–8132. [PubMed: 16834198]

Chen X, Tureček F. The arginine anomaly: arginine radicals are poor hydrogen atom donors in electron transfer induced dissociations. J. Am. Chem. Soc. 2006; 128:12520–12530. [PubMed: 16984203]

Chen Y-L, Collings BA, Douglas DJ. Collision cross sections of myoglobin and cytochrome *c* ions with Ne, Ar, and Kr. J. Am. Soc. Mass Spectrom. 1997; 8:681–687.

Clowers BH, Ibrahim YM, Prior DC, Danielson WF, Belov ME, Smith RD. Enhanced ion utilization efficiency using an electrodynamic ion funnel trap as an injection mechanism for ion mobility spectrometry. Anal. Chem. 2008; 80:612–623. [PubMed: 18166021]

Creaser CS, Ratcliffe L. Atmospheric pressure matrix-assisted laser desorption/ionisation mass spectrometry: A review. Curr. Anal. Chem. 2006; 2:9–15.

Dehmelt HG. Radiofrequency spectroscopy of stored ions. Adv. Atom. Mol. Phys. 1967; 3:53–72.

Dodonov A, Kozlovsky V, Loboda A, Raznikov V, Sulimenkov I, Tolmachev A, Kraft A, Wollnik H. A new technique for decomposition of selected ions in molecule ion reactor coupled with ortho-time-of-flight mass spectrometry. Rapid Commun. Mass Spectrom. 1997; 11:1649–1656. [PubMed: 9364793]

Douglas DJ, French JB. Gas dynamics of the inductively coupled plasma mass spectrometry interface. J. Anal. At. Spectrom. 1988; 3:743–747.

Douglas DJ, French JB. Collisional focusing effects in radio-frequency quadrupoles. J. Am. Soc. Mass Spectrom. 1992; 3:398–408.

Eliseev SA, Block M, Chaudhuri A, Di Z, Habs D, Herfurth F, Kluge H-J, Neumayr JB, Plaß WR, Rauth C, Thirolf PG, Vorobjev G, Wang Z. Extraction efficiency and extraction time of the SHIPTRAP gas-filled stopping cell. Nuclear Instruments & Methods in Physics Research B. 2007; 258:479–484.

Fenn JB, Mann M, Meng CK, Wong SF, Whitehouse CM. Electrospray ionization-principles and practice. Mass Spectrom. Rev. 1990; 9:37–70.

Flora JW, Hannis JC, Muddiman DC. High-mass accuracy of product ions produced by SORI-CID using a dual electrospray ionization source coupled with FTICR mass spectrometry. Anal. Chem. 2001; 73:1247–1251. [PubMed: 11305659]

Fuh M-R, Hsieh C-J. Determination of flunarizine in rat brain by liquid chromatography-electrospray mass spectrometry. J. Chromatogr. B. 1999; 736:167–173.

Gale DC, Smith RD. Small volume and low flow-rate electrospray ionization mass spectrometry of aqueous samples. Rapid Commun. Mass Spectrom. 1993; 7:1017–1021.

Gamero-Castaño M, Aguirre-de-Carcer I, de Juan L, de la Mora J Fernández. On the current emitted by Taylor cone-jets of electrolytes in vacuo: Implications for liquid metal ion sources. J. Appl. Phys. 1998; 83:2428–2434.

Gerlich, D. Inhomogeneous rf fields: A versatile tool for the study of processes with slow ions. In: Ng, C-Y.; Baer, M., editors. State-Selected and State-to-State Ion-Molecule Reaction Dynamics. Part 1. Experiment. Wiley; New York: 1992. p. 1-176.Advances in Chemical Physics Series 82

Gidden J, Baker ES, Ferzoco A, Bowers MT. Structural motifs of DNA complexes in the gas phase. Int. J. Mass Spectrom. 2005; 240:183–193.

Gidden J, Ferzoco A, Baker ES, Bowers MT. Duplex formation and the onset of helicity in poly $d(CG)_n$ oligonucleotides in a solvent-free environment. J. Am. Chem. Soc. 2004; 126:15132–15140. [PubMed: 15548010]

Hannis JC, Muddiman DC. A dual electrospray ionization source combined with hexapole accumulation to achieve high mass accuracy of biopolymers in fourier transform ion cyclotron

resonance mass spectrometry. J. Am. Soc. Mass Spectrom. 2000; 11:876–883. [PubMed: 11014449]

Heinz S, Äystö J, Habs D, Hegewisch S, Huikari J, Nieminen A, Rinta-Antila S, Schumann M, Szerypo J. A radio frequency ring electrode cooler for low-energy ion beams. Nuclear Instruments & Methods in Physics Research A. 2004; 533:239–247.

Ibrahim Y, Tang K, Tolmachev AV, Shvartsburg AA, Smith RD. Improving mass spectrometer sensitivity using a high-pressure electrodynamic ion funnel interface. J. Am. Soc. Mass Spectr. 2006; 17:1299–1305.

Ibrahim Y, Belov ME, Tolmachev AV, Prior DC, Smith RD. Ion funnel trap interface for orthogonal time-of-flight mass spectrometry. Anal. Chem. 2007; 79:7845–7852. [PubMed: 17850113]

Ibrahim YM, Belov ME, Liyu AV, Smith RD. Automated gain control ion funnel trap by orthogonal time-of-flight mass spectrometry. Anal. Chem. 2008; 80:5367–5376. [PubMed: 18512944]

Inatsugu, N.; Waki, H. Mass Spectrometer. US Patent. 6,462,338 B1. 2002.

Jones JW, Sasaki T, Goodlett DR, Tureček F. Electron capture in spin-trap capped peptides. An experimental example of ergodic dissociation in peptide cation-radicals. J. Am. Soc. Mass Spectrom. 2007; 18:432–444. [PubMed: 17112737]

Julian RR, Mabbett SR, Jarrold MF. Ion funnels for the masses: Experiments and simulations with a simplified ion funnel. J. Am. Soc. Mass Spectrom. 2005; 16:1708–1712. [PubMed: 16095911]

Kast J, Gentzel M, Wilm M, Richardson K. Noise filtering techniques for electrospray quadrupole time of flight mass spectra. J. Am. Soc. Mass Spectrom. 2003; 14:766–776. [PubMed: 12837599]

Kelly RT, Page JS, Luo Q, Moore RJ, Orton DJ, Tang K, Smith RD. Chemically etched open tubular and monolithic emitters for nanoelectrospray ionization mass spectrometry. Anal. Chem. 2006; 78:7796–7801. [PubMed: 17105173]

Kelly RT, Page JS, Tang K, Smith RD. Array of chemically etched fused-silica emitters for improving the sensitivity and quantitation of electrospray ionization mass spectrometry. Anal. Chem. 2007; 79:4192–4198. [PubMed: 17472340]

Kelly RT, Page JS, Marginean I, Tang K, Smith RD. Nanoelectrospray emitter arrays providing inter-emitter electric field uniformity. Anal. Chem. 2008a; 80:5660–5665. [PubMed: 18553942]

Kelly RT, Page JS, Zhao R, Qian W-J, Mottaz HM, Tang K, Smith RD. Capillary-based multi nanoelectrospray emitters: Improvements in ion transmission efficiency and implementation with capillary reversed-phase LC-ESI-MS. Anal. Chem. 2008b; 80:143–149. [PubMed: 18044958]

Kim T, Tolmachev AV, Harkewicz R, Prior DC, Anderson GA, Udseth HR, Smith RD, Bailey TH, Rakov S, Futrell JH. Design and implementation of a new electrodynamic ion funnel. Anal. Chem. 2000a; 72:2247–2255. [PubMed: 10845370]

Kim T, Udseth HR, Smith RD. Improved ion transmission from atmospheric pressure to high vacuum using a multi-capillary inlet and electrodynamic ion funnel interface. Anal. Chem. 2000b; 72:5014–5019. [PubMed: 11055723]

Kim T, Tang K, Udseth HR, Smith RD. A multicapillary inlet jet disruption electrodynamic ion funnel interface for improved sensitivity using atmospheric pressure ion sources. Anal. Chem. 2001; 73:4162–4170. [PubMed: 11569805]

Kitching KJ, Lee H-N, Elam WT, Johnston EE, MacGregor H, Miller RJ, Tureček F, Ratner BD. Development of an electrospray approach to deposit complex molecules on plasma modified surfaces. Rev. Sci. Inst. 2003; 74:4832–4839.

Koeniger SL, Merenbloom SI, Valentine SJ, Jarrold MF, Udseth HR, Smith RD, Clemmer DE. An IMS—IMS analogue of MS—MS. Anal. Chem. 2006; 78:4161–4174. [PubMed: 16771547]

Lin B, Sunner J. Ion transport by viscous gas flow through capillaries. J. Am. Soc. Mass Spectrom. 1994; 5:873–885.

Liu D, Wyttenbach T, Bowers MT. Hydration of mononucleotides. J. Am. Chem. Soc. 2006; 128:15155–15163. [PubMed: 17117867]

Liu T, Belov ME, Jaitly N, Qian W-J, Smith RD. Accurate mass measurements in proteomics. Chem. Rev. 2007; 107:3621–3653. [PubMed: 17649984]

Lynn EC, Chung M-C, Han C-C. Characterizing the transmission properties of an ion funnel. Rapid Commun. Mass Spectrom. 2000; 14:2129–2134. [PubMed: 11114020]

Mayer PS, Tureček F, Lee H-N, Scheidemann AA, Olney TN, Schumacker F, Štrop P, Smrčina M, Pátek M, Schirlin D. Preparative separation of mixtures by mass spectrometry. Anal. Chem. 2005; 77:4378–4384. [PubMed: 16013849]

Merenbloom SI, Koeniger SL, Valentine SJ, Plasencia MD, Clemmer DE. IMS-IMS and IMS-IMS-IMS/MS for separating peptide and protein fragment ions. Anal. Chem. 2006; 78:2802–2809. [PubMed: 16615796]

Moision RM, Armentrout PB. An electrospray ionization source for thermochemical investigation with the guided ion beam mass spectrometer. J. Am. Soc. Mass Spectrom. 2007; 18:1124–1134. [PubMed: 17462909]

Neumayr JB, Beck L, Habs D, Heinz S, Szerypo J, Thirolf PG, Varentsov V, Voit F, Ackermann D, Beck D, Block M, Di Z, Eliseev SA, Geissel H, Herfurth F, Heßberger FP, Hofmann S, Kluge H-J, Mukherjee M, Münzenberg G, Petrick M, Quint W, Rahaman S, Rauth C, Rodríguez D, Scheidenberger C, Sikler G, Wang Z, Weber C, Plaß WR, Breitenfeldt M, Chaudhuri A, Marx G, Schweikhard L, Dodonov AF, Novikov Y, Suhonen M. The ion-catcher device for SHIPTRAP. Nuclear Instruments and Methods in Physics Research B. 2006a; 244:489–500.

Neumayr JB, Thirolf PG, Habs D, Heinz S, Kolhinen VS, Sewtz M, Szerypo J. Performance of the MLL-IonCatcher. Rev. Sci. Instrum. 2006b; 77:065109.

Page JS, Bogdanov B, Vilkov AN, Prior DC, Buschbach MA, Tang K, Smith RD. Automatic gain control in mass spectrometry using a jet disrupter electrode in an electrodynamic ion funnel. J. Am. Soc. Mass Spectrom. 2005a; 16:244–253. [PubMed: 15694774]

Page JS, Tolmachev AV, Tang K, Smith RD. Variable low-mass filtering using an electrodynamic ion funnel. J. Mass Spectrom. 2005b; 40:1215–1222. [PubMed: 16127660]

Page JS, Tolmachev AV, Tang K, Smith RD. Theoretical and experimental evaluation of the low m/z transmission of an electrodynamic ion funnel. J. Am. Soc. Mass Spectrom. 2006; 17:586–592. [PubMed: 16503158]

Page JS, Tang K, Smith RD. An electrodynamic ion funnel interface for greater sensitivity and higher throughput with linear ion trap mass spectrometers. Int. J. Mass Spectrom. 2007; 265:244–250.

Page JS, Tang K, Kelly RT, Smith RD. Subambient pressure ionization with nanoelectrospray source and interface for improved sensitivity in mass spectrometry. Anal. Chem. 2008a; 80:1800–1805. [PubMed: 18237189]

Page, JS.; Tang, K.; Kelly, RT.; Smith, RD. A new ionization source for mass spectrometry: Subambient pressure ionization with nanoelectrospray (SPIN). 56th ASMS Conference on Mass Spectrometry and Allied Topics; Denver, CO. 2008b.

Roach, P.; Kuchta, K.; Woodward, W.; Castleman, AW. Efficiently transporting ions from viscous flow to ultra-high vacuum with minimal loss. 56th ASMS Conference on Mass Spectrometry and Allied Topics; Denver, CO. 2008.

Rulison AJ, Flagan RC. Scale-up of electrospray atomization using linear arrays of Taylor cones. Rev. Sci. Instrum. 1993; 64:683–686.

Seymour JL, Syrstad EA, Langley CC, Tureček F. Neutralization-reionization of ions produced by electrospray. Instrument design and initial data. Int. J. Mass Spectrom. 2003; 228:687–702.

Shaffer SA, Tang K, Anderson GA, Prior DC, Udseth HR, Smith RD. A novel ion funnel for focusing ions at elevated pressure using electrospray ionization mass spectrometry. Rapid Commun. Mass Spectrom. 1997; 11:1813–1817.

Shaffer SA, Prior DC, Anderson GA, Udseth HR, Smith RD. An ion funnel interface for improved ion focusing and sensitivity using electrospray ionization mass spectrometry. Anal. Chem. 1998; 70:4111–4119. [PubMed: 9784749]

Shaffer SA, Tolmachev A, Prior DC, Anderson GA, Udseth HR, Smith RD. Characterization of a new electrodynamic ion funnel interface for electrospray ionization mass spectrometry. Anal. Chem. 1999; 71:2957–2964. [PubMed: 10450147]

Shwartz, JC.; Zhou, X-G.; Bier, ME. Method and apparatus of increasing dynamic range and sensitivity of a mass spectrometer. US Patent. 5,572,022. 1996.

Smith RD, Shen Y, Tang K. Ultrasensitive and quantitative analyses from combined separations—mass spectrometry for the characterization of proteomes. Acc. Chem. Res. 2004; 37:269–278. [PubMed: 15096064]

Takats Z, Wiseman JM, Gologan B, Cooks RG. Mass spectrometry sampling under ambient conditions with desorption electrospray ionization. Science. 2004; 306:471–473. [PubMed: 15486296]

Tang K, Lin Y, Matson DW, Kim T, Smith RD. Generation of multiple electrosprays using microfabricated emitter arrays for improved mass spectrometric sensitivity. Anal. Chem. 2001; 73:1658–1663. [PubMed: 11338576]

Tang K, Tolmachev AV, Nikolaev E, Zhang R, Belov ME, Udseth HR, Smith RD. Independent control of ion transmission in a jet disrupter dual-channel ion funnel electrospray ionization MS interface. Anal. Chem. 2002; 74:5431–5437. [PubMed: 12403604]

Tang K, Shvartsburg AA, Lee H-N, Prior DC, Buschbach MA, Li F, Tolmachev A, Anderson GA, Smith RD. High-sensitivity ion mobility spectrometry/mass spectrometry using electrodynamic ion funnel interfaces. Anal. Chem. 2005; 77:3330–3339. [PubMed: 15889926]

Tejeda G, Maté B, Fernández-Sánchez JM, Montero S. Temperature and density mapping of supersonic jet expansions using linear raman spectroscopy. Phys. Rev. Lett. 1996; 76:34–37. [PubMed: 10060427]

Thomson BA. 1997 McBryde Medal Award Lecture - Radio frequency quadrupole ion guides in modern mass spectrometry. Can. J. Chem. 1998; 76:499–505.

Tolmachev AV, Chernushevich IV, Dodonov AF, Standing KG. A collisional focusing ion guide for coupling an atmospheric pressure ion source to a mass spectrometer. Nuclear Instruments and Methods in Physics Research B. 1997; 124:112–119.

Tolmachev AV, Kim T, Udseth HR, Smith RD, Bailey TH, Futrell JH. Simulation-based optimization of the electrodynamic ion funnel for high sensitivity electrospray ionization mass spectrometry. Int. J. Mass Spectrom. 2000; 203:31–47.

Varentsov VL, Habs D. A cooler for intense low-energy ion beams. Nuclear Instruments and Methods in Physics Research. 2002; 490:16–29.

Volný M, Elam WT, Branca A, Ratner BD, Tureček F. Preparative soft and reactive landing of multiply charged protein ions on a plasma-treated metal surface. Anal. Chem. 2005; 77:4890–4896. [PubMed: 16053302]

Volný M, Tureček F. High efficiency in soft landing of biomolecular ions on a plasma-treated metal surface: Are double-digit yields possible? J. Mass Spectrom. 2006; 41:124–126. [PubMed: 16317712]

Volný M, Sengupta A, Wilson CB, Swanson BD, Davis EJ, Tureček F. Surface-enhanced raman spectroscopy of soft-landed polyatomic ions and molecules. Anal. Chem. 2007; 79:4543–4551. [PubMed: 17503769]

Wilm MS, Mann M. Electrospray and Taylor-Cone Theory, Dole's beam of macromolecules at last? Int. J. Mass Spectrom. Ion Processes. 1994; 136:167–180.

Wouters, ER.; Splendore, M.; Senko, MW.; Syka, JEP.; Dunyach, J-J. Design of a progressively spaced stacked ring ion guide for improved ion transmission at high pressure. 56th ASMS Conference on Mass Spectrometry and Allied Topics; Denver, CO. 2008.

Wyttenbach T, Kemper PR, Bowers MT. Design of a new electrospray ion mobility mass spectrometer. Int. J. Mass Spectrom. Ion Processes. 2001; 212:13–23.

Yao C, Cuadrado-Peinado ML, Polášek M, Tureček F. Specific generation of 1-methylcytosine radicals in the gas phase. Angew. Chem. Int. Ed. 2005; 44:6708–6711.

Yao C, Syrstad EA, Tureček F. Electron transfer to protonated β-alanine N-methylamide in the gas phase: An experimental and computational study of dissociation energetics and mechanisms. J. Phys. Chem. A. 2007; 111:4167–4180. [PubMed: 17455922]

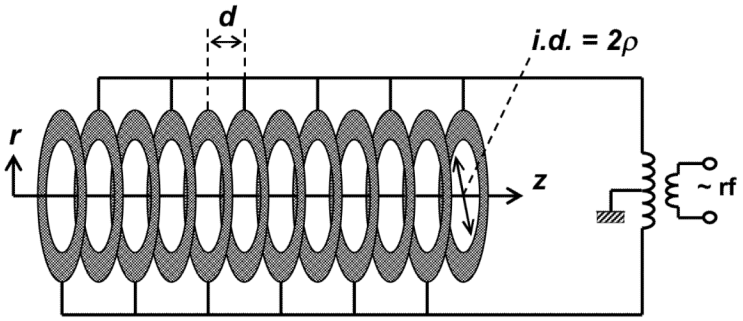

Figure 1.
Diagram of a stacked ring rf ion guide.

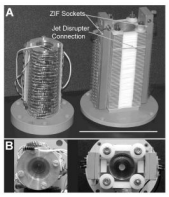

Figure 2.
Ion funnel photographs. (A) Side-view images of the original 28 electrode prototype (left) and a currently used 100 electrode design with jet disrupter (right). Scale bar is 100 mm. (B) Corresponding top-view images. The jet disrupter electrode can be seen in the current design (right).

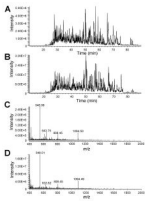

Figure 3.
Base peak chromatograms from the LC—MS analysis of a global tryptic digest of *S. oneidensis* using the standard instrument interface (A) and the ion funnel interface (B). Representative mass spectra from (A) and (B) are shown in (C) and (D), respectively. Adapted with permission from (Page et al., 2007).

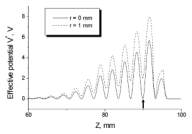

Figure 4.

Effective rf potential along the ion funnel central (*z*) axis for the ion funnel prototype developed by Shaffer, et al. (1999). The effective potential is calculated according to equation (1), using numerically computed electric field intensity. The parameters are: *m/z = 1000, V_{rf} =100 V*, rf frequency = 700 kHz. The axial interval shown corresponds to the final 11 ring electrodes of the ion funnel and the 1-mm-i.d. conductance limit located at *z = 96mm*. The axial position of the largest axial well is indicated by the arrow. Adapted with permission from (Shaffer et al., 1999).

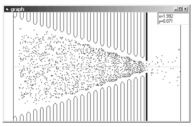

Figure 5.

Screen capture of the ion funnel computer model simulation for the design of Kim, et al. (Kim, et al., 2000a). V_{pp} = 200V; frequency = 0.7 MHz; dc gradient = 30 V/cm; input current = 8 nA; m/z = 1000. Exit configuration: final rf ring = 2 mm i.d.; dc-only conductance limit (1.5 mm) positioned 0.5 mm from the final rf ring.

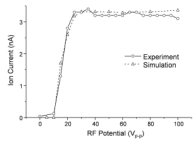

Figure 6.

Experimental (circles) and simulated (triangles) dependence of ion transmission on rf potential for gramicidin ions using the 100 electrode ion funnel design (Kim, et al., 2000a). The ion current was measured after the ion funnel exit for P = 1 Torr; input current = 5 nA; frequency = 0.7 MHz; axial dc field = 16 V/cm. Simulations used the same conditions. Adapted with permission from (Tolmachev et al., 2000).

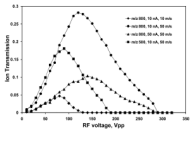

Figure 7.

Ion transmission efficiency vs. rf voltage simulated using the computer model of the progressively spaced stacked ring ion guide. The ion *m/z*, current, and initial velocity corresponding to each curve are shown in the figure. The modeled configuration consisted of 11 ring rf electrodes, 5 mm i.d., with the spacing progressively increasing from 2 to 5 mm. The exit DC-only ring electrode, 2 mm i.d., is positioned 1.5 mm from the final rf ring electrode. The rf frequency was 700 kHz, gas pressure was 1 Torr (N_2), and a uniform gas flow along z-axis was assumed. The initial ion cloud was 2.5 mm in diameter.

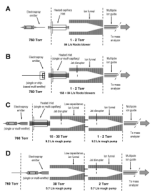

Figure 8.
Drawings of various ESI/ion funnel interfaces. (A) The initial ion funnel design (Shaffer et al., 1998), using single capillary inlets and high-speed pumps. (B) Implementation of multiple heated inlet capillaries (Kim et al., 2000b), which increased ion transmission but also increased the pumping requirements, even when a jet disrupter electrode was used. (C) Higher pressure ion funnel operated in tandem with a standard ion funnel (Ibrahim et al., 2006). The additional pumping stage enables the use of low-speed pumps. (D) A low pressure ESI interface, in which the electrospray source sprays directly into an ion funnel, eliminating the transmission losses that normally occur at the inlet (Page et al., 2008b).

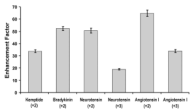

Figure 9.

Sensitivity enhancements afforded by the use of a linear array of 19 emitters, a multi-capillary heated inlet, and high-pressure ion funnel interface compared with the commercial instrument configuration (Kelly et al., 2008a). The peptides in the mixture each had a concentration of 500 nM and the solution flow rate was 2 μL/min.

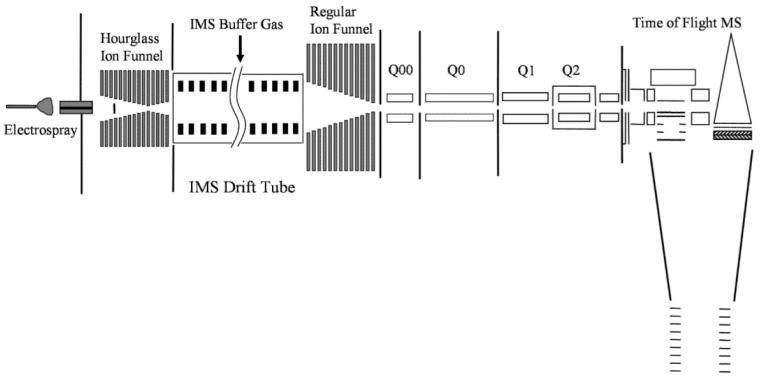

Figure 10.
Schematic of the ESI-IMS-QTOF instrument with ion funnels at the entrance and exit of the ion mobility drift tube. Adapted with permission from (Tang et al., 2005).

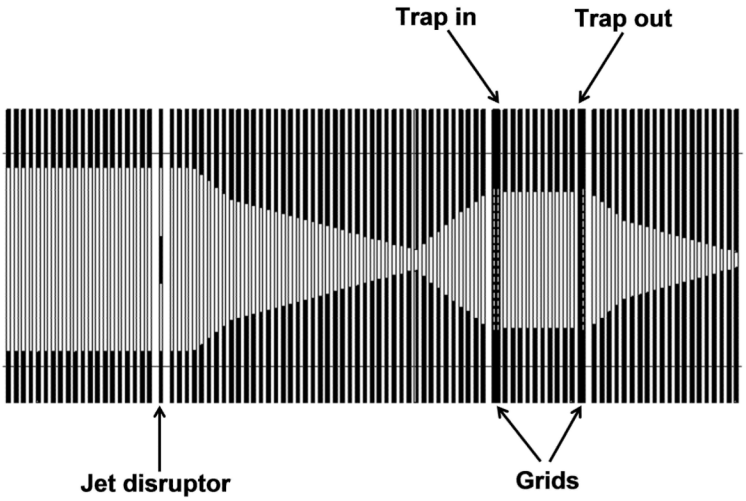

Figure 11.
Diagram of an ion funnel trap. Adapted with permission from (Ibrahim et al., 2007).